催 化 学 报
2012 Chinese Journal of Catalysis Vol. 33 No. 5

文章编号: 0253-9837(2012)05-0802-06 国际版 DOI: 10.1016/S1872-2067(11)60380-X 研究论文: 802~807

硫化亚铜/四针状氧化锌晶须纳米复合材料的制备及其光催化性能

吴德智, 范希梅*, 代 佳, 刘花蓉, 刘 红, 张冯章

西南交通大学材料科学与工程学院, 材料先进技术教育部重点实验室, 四川成都 610031

摘要: 在聚乙烯吡咯烷酮的辅助下, 采用多元醇法制备了不同铜/锌摩尔比的硫化亚铜/四针状氧化锌晶须纳米复合材料, 并利用 X 射线衍射、场发射扫描电镜、X 射线光电子能谱和紫外-可见漫反射光谱对样品进行了表征. 结果表明, 在紫外光照射下, 样品对甲基橙的光降解效率优于纯 ZnO 晶须. 在铜/锌摩尔比低于 4% 时, 样品的光催化性能随着铜/锌摩尔比增加而增加, 但随着铜/锌摩尔比的继续增加, 样品的光催化性能下降. 此外, 还采用周期实验来评价催化剂的稳定性. 结果表明, 该催化剂具有优异的光催化稳定性.

关键词: 氧化锌; 硫化亚铜; 多元醇法; 光催化性能; 甲基橙

中图分类号: O643 **文献标识码**: A

收稿日期: 2011-12-09. 接受日期: 2012-02-27.

*通讯联系人. 电话: (028)87602714; 传真: (028)87600454; 电子信箱: fanximei@126.com

基金来源: 国家高技术研究发展计划 (863 计划, 2009AA03Z427); 四川省科学基金 (2006z02-006-3).

本文的英文电子版(国际版)由Elsevier出版社在ScienceDirect上出版(http://www.sciencedirect.com/science/journal/18722067).

Preparation and Photocatalytic Properties of Cu_2S/Tetrapod-Like ZnO Whisker Nanocomposites

WU Dezhi, FAN Ximei*, DAI Jia, LIU Huarong, LIU Hong, ZHANG Fengzhang

Key Laboratory of Advanced Technologies of Materials, Ministry of Education, School of Materials Science and Engineering, Southwest Jiaotong University, Chengdu 610031, Sichuan, China

Abstract: Nanocomposites of tetrapod-like ZnO whisker (T-ZnOw) with loaded Cu_2S were synthesized with different Cu/Zn molar ratios with the assistant of poly(vinyl pyrrolidone) (PVP) by the polyol process. The composite samples were characterized by X-ray diffraction, field emission scanning electron microscopy, X-ray photoelectron spectroscopy, and UV-visible diffuse reflectance spectroscopy. The photocatalytic activities for the Cu_2S/T-ZnOw nanocomposites increased with Cu/Zn molar ratio up to 4%, and then decreased with further increase of the Cu/Zn molar ratio up to 10%. The Cu_2S/T-ZnOw nanocomposites exhibited higher activity than T-ZnOw for the photocatalytic degradation of methyl orange. Recycling experiments were also performed. The photocatalytic activity of the photocatalyst showed no decrease after three cycles, which demonstrated that the Cu_2S/T-ZnOw photocatalyst had excellent stability.

Key words: zinc oxide; copper sulphide; polyol method; photocatalytic performance; methyl orange

Received 9 December 2011. Accepted 27 February 2012.

**Corresponding author. Tel: +86-28-87602714; Fax: +86-28-87600454; E-mail: fanximei@126.com*

This work was supported by the National High Technology Research and Development Program of China (863 Program, 2009AA03Z427) and the Science Foundation of Sichuan Province (2006z02-006-3).

English edition available online at Elsevier ScienceDirect (http://www.sciencedirect.com/science/journal/18722067).

Semiconducting zinc oxide (ZnO) can be used for the purification of environmental pollutants due to its optical properties [1–5]. The effects of its morphology on photocatalytic property have been investigated in detail [6–9]. The rapid recombination of photogenerated electron (e^-)-hole (h^+) pairs is the major factor limiting its widespread use in environmental purification [10]. An improvement in the separation efficiency of photogenerated electrons and holes in ZnO is important to solve this. The charge separation efficiency can be enhanced by using cou-

pled semiconductor materials with different band gap energy levels, and coupled semiconductor photocatalysts have exhibited higher photocatalytic activities than single semiconductor photocatalysts. There are a number of studies on the photocatalytic activity of ZnO coupled with a metal oxide, e.g., SnO_2 [11,12], WO_3 [13], Fe_2O_3 [14,15], or CdS [16]. The coupling of different semiconductor oxides achieves a more efficient charge separation and enhanced photocatalytic performance by the transfer of the charge carriers (electrons and holes) produced under irradiation from one semiconductor to the other [17,18]. Cu_2S is a p-type semiconductor material with a bulk band gap in range of 1.22–1.24 eV and the conduction and valence band positions of Cu_2S are above that of ZnO [19,20], which are beneficial for the separation of photogenerated electrons and holes.

The aim of this study is to optimize the preparation of coupled Cu_2S/T-ZnOw nanocomposites and to investigate the role of Cu_2S in enhancing the photocatalytic properties of ZnO. Cu_2S/tetrapod-like ZnO whisker (T-ZnOw) nanocomposites were synthesized by the polyol method with different Cu/Zn molar ratios with the assistant of poly(vinyl pyrrolidone) (PVP). The effects of Cu/Zn molar ratio on the morphology and photocatalytic property of the Cu_2S/T-ZnOw nanocomposites are discussed.

1 Experimental

1.1 Polyol synthesis of Cu_2S/T-ZnOw nanocomposites

T-ZnOw was prepared by the equilibrium gas expanding method at 700 °C with metallic zinc as the raw material, which was reported in detail in our previous work [21]. Cu_2S/T-ZnOw nanocomposites were synthesized by the polyol method with different Cu/Zn molar ratios (2%–10%) using copper acetate (analytical grade), PVP, thiourea, diethylene glycol (DEG), and T-ZnOw. The preparation procedure was as follows. First, a known amount of copper acetate (0.2, 0.4, 0.6, 0.8, and 1.0 g) was added into 80 ml of DEG with a PVP concentration of 5 g/L. The solution was magnetically stirred for about 30 min. Then, 2 g T-ZnOw was poured into the above solution. Subsequently, 20 ml solution of thiourea (0.005, 0.01, 0.015, 0.02, and 0.025 mol/L) was slowly dropped into the above mixed solution. The mixed suspension was maintained at 180 ºC for 30 min. After cooling to room temperature in air, the precipitate was separated from the solution by centrifugation, then washed with distilled water and absolute alcohol three times, and finally dried in a vacuum oven at 60 ºC for 8 h. Cu_2S/T-ZnOw nanocomposites were obtained.

1.2 Characterization

The structure analysis was performed by X-ray diffraction (Panalytical X'pert PRO) with a Cu target and a monochromator at 40 kV and 40 mA. Field emission scanning electron microscopy (FE-SEM, Fei Inspect) with an accelerating voltage of 10 kV was conducted to analyze the morphology of the photocatalysts. Energy dispersive X-ray spectroscopy (EDS) attached to the FE-SEM instrument was used to determine the chemical compositions of the samples. X-ray photoelectron spectroscopy (XPS) was performed with a PHI 5600 multi-technique system with a monochromatic Al K_α X-ray source. All core level spectra were referenced to the C 1*s* neutral carbon peak at 284.8 eV. UV-visible diffuse reflectance spectroscopy (UV-Vis DRS) with a Lambda 900 UV-Vis spectrometer was performed to analyze the optical absorption property of the samples.

1.3 Photocatalytic activity

The photocatalytic activity was evaluated by the photodegradation of methyl orange (MO) under UV light irradiation (λ = 254 nm) at 25 ºC in a homemade apparatus. First, 50 mg photocatalysts with different Cu/Zn molar ratios were added into five beakers filled with 50 ml of MO aqueous solution (10 mg/L). The suspensions were magnetically stirred in the dark for 20 min, and subsequently irradiated by a UV-lamp at 254 nm emission wavelength. The solution was sampled every 20 min during UV irradiation to determine the degradation efficiency of MO, which was done by measuring the absorbance at 466 nm using a UV-Vis 2550 spectrophotometer. To further investigate the stability of the Cu_2S/T-ZnOw, recycling experiments for the photodegradation of MO were also performed.

2 Results and discussion

2.1 Structure and surface morphology

Figure 1 shows the XRD patterns of Cu_2S, T-ZnO whiskers, and Cu_2S/T-ZnOw nanocomposites with different Cu/Zn molar ratios. The characteristic peaks marked by the black circles are from the (111), (200), (220), and (311) crystal planes of the Cu_2S cubic phase (JCPDS 84-1770). The XRD patterns of ZnO and Cu_2S/T-ZnOw nanocomposites exhibited the characteristic peaks for the wurtzite structure of ZnO. This indicated the crystal structure of ZnO was not modified during the synthesis of the nanocomposite particles. However, the peaks of Cu_2S were absent in the Cu_2S/T-ZnOw nanocomposite patterns, which may be attributed to the very low amount of Cu_2S on the surface of T-ZnOw, and the characteristic diffraction peaks of ZnO were too strong to allow seeing the diffraction peaks of Cu_2S.

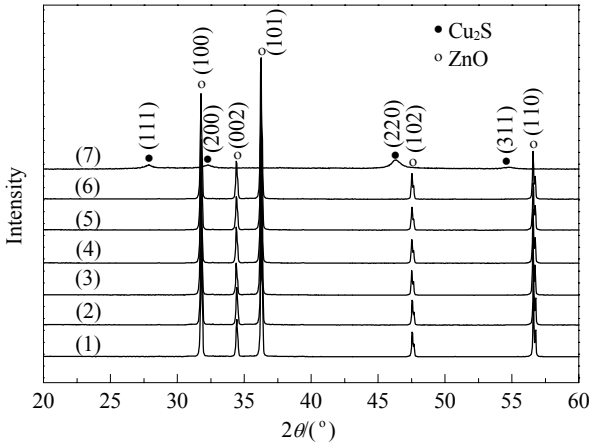

Fig. 1. XRD patterns of different samples. (1) T-ZnOw; (2) 2% Cu_2S/T-ZnOw; (3) 4% Cu_2S/T-ZnOw; (4) 6% Cu_2S/T-ZnOw; (5) 8% Cu_2S/T-ZnOw; (6) 10% Cu_2S/T-ZnOw; (7) Cu_2S.

Figure 2 shows the SEM images of T-ZnOw and Cu_2S/T-ZnOw nanocomposites. Figure 2(a) gives the surface morphology of T-ZnOw with arms about 20–40 μm long. Figure 2(b–f) shows the FE-SEM characterization of the morphology of the Cu_2S/T-ZnOw nanocomposites with Cu/Zn molar ratio of 2%–10%. For all the Cu_2S/T-ZnOw nanocomposites, many nanoparticles were dispersed on the surface of T-ZnOw and the number of nanoparticles increased with increasing Cu/Zn molar ratio. As shown in Fig. 2(b) and (c), when the Cu/Zn molar ratio was in the range of 2%–4%, the nanoparticles were uniformly deposited on the surface of T-ZnOw. Some nanoparticles aggregated into microscaled agglomerates on the surface of T-ZnOw with the further increase of the Cu/Zn molar ratio to 6%–10% (shown in Fig. 2(d–f)).

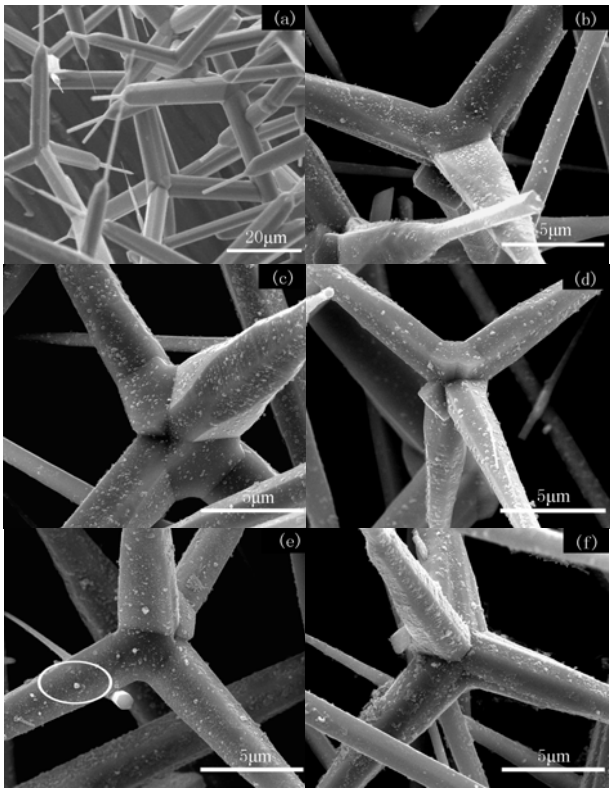

Fig. 2. FE-SEM images of T-ZnOw and Cu_2S/T-ZnOw photocatalysts. (a) T-ZnOw; (b) 2% Cu_2S/T-ZnOw; (c) 4% Cu_2S/T-ZnOw; (d) 6% Cu_2S/T-ZnOw; (e) 8% Cu_2S/T-ZnOw; (f) 10% Cu_2S/T-ZnOw.

The chemical compositions of the nanoparticles on the surface of T-ZnOw were determined by EDS analysis. As shown in Fig. 2(e), in an area where nanoparticles were deposited on the surface which was marked by the white circle, the corresponding EDS spectra included the peaks of Zn, O, Cu, and S (shown in Fig. 3). The result showed that the nanoparticles were composed of Cu and S. Their chemical states were determined by XPS analysis. It is well known that the organic surfactants can sufficiently disperse clusters of particles to give monodispersed particles and they have the ability to determine not only the shape but also the size of the particles [22]. As an organic surfactant, PVP has been reported to play an important role in the fabrication of nanomaterials, and it can act as a size-control agent or shape-directing agent [23,24]. In this work, an increase of Cu/Zn molar ratio also meant a decrease of the PVP content. So, large agglomerates gradually appeared as the Cu/Zn molar ratio increased.

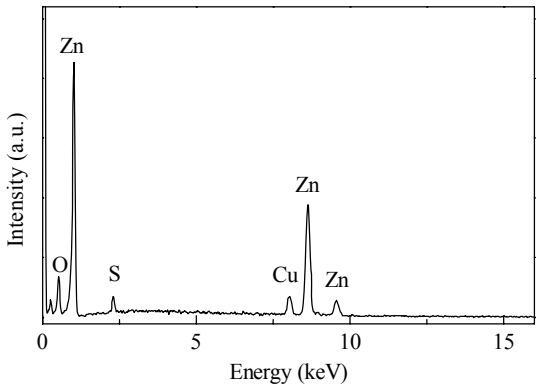

Fig. 3. EDS spectrum of 8% Cu_2S/T-ZnOw.

2.2 XPS and UV-Vis DRS analysis

To further investigate the surface chemical states of the photocatalyst, XPS analysis was performed. The XPS spectrum of the Cu_2S/T-ZnOw photocatalyst with 4% Cu/Zn molar ratio is shown in Fig. 4. Figure 4(a) gives the whole spectrum of the photocatalyst, which only exhibited the peaks of Zn, O, Cu, and S, and indicated that the photocatalyst was composed of Zn, O, Cu, and S species. The XPS spectrum for Cu 2*p* is shown in Fig. 4(b). The binding energies of Cu $2p_{3/2}$ and Cu $2p_{1/2}$ were located at 932.3 and 952.3 eV, respectively, which is consistent with the standard

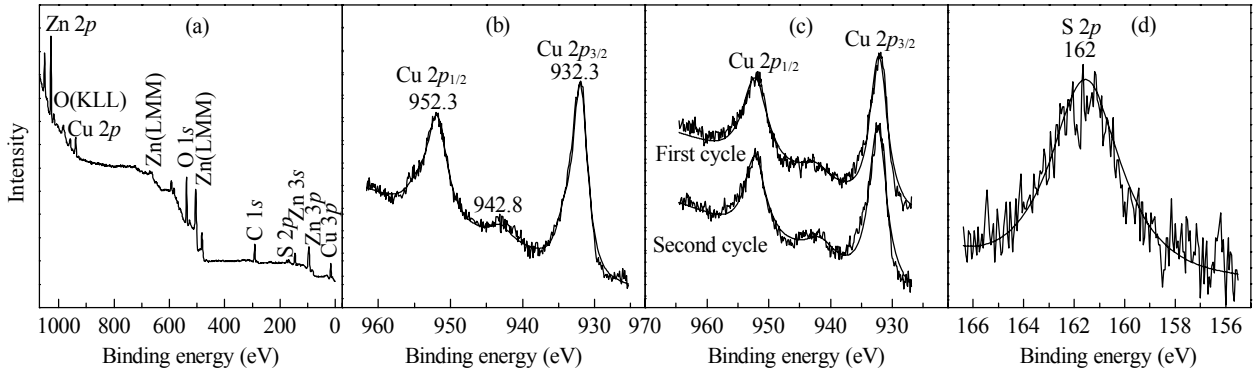

Fig. 4. XPS profiles of the 4% Cu_2S/T-ZnOw photocatalyst. (a) Full spectrum; (b) Spectrum for Cu 2*p*; (c) Spectra for Cu 2*p* after the recycling experiment; (d) Spectrum for S 2*p*.

reference for the XPS spectrum of Cu^+ [25,26]. In addition, the observed "shake-up" feature associated with the Cu 2*p* line located at about 942.8 eV can be assigned to the Cu^{2+} oxidation state [27,28]. The result demonstrated that the surface of Cu_2S was partially oxidized. The oxidized amount calculated by XPS was 4.36%, which is relatively low. Figure 4(c) shows the spectra of Cu 2*p* after the recycling experiments. The characteristic "shake-up" peak of Cu 2*p* line showed little change after the first and second cycles, which indicated that the sample was oxidized slightly after the recycling experiment. The oxidized amounts were also quantitatively analyzed by XPS and the oxidized percentages after the first and second cycles were 4.83% and 5.61%, respectively. This showed the Cu_2S/T-ZnOw photocatalyst possessed excellent stability. Figure 4(d) shows that the binding energy of S 2*p* for the photocatalyst was 162 eV, which is lower than that of sulfur and related compounds (S^0: 164.0 eV; chemisorbed SO_2: 163–165.5 eV; SO_3^{2-}: 166.4 eV; SO_4^{2-}: 168–170 eV), and corresponded to the S^{2-} state [29]. The XPS analysis demonstrated that Cu_2S nanoparticles were successfully grown on the surface of T-ZnOw. The growth mechanism for Cu_2S nanomaterials was probably the following [30]: $Cu^{2+} + (CH_2{=}CHCHOH)_2 \rightarrow Cu^+ + CH_2{=}CHCOCHOHCH{=}CH_2 + H^+$, $2Cu^+ + S^{2-} \rightarrow Cu_2S$. Under the experimental conditions, DEG reduced Cu^{2+} ion from $Cu(CH_3COO)_2$ to Cu^+ ion and then the Cu^+ ion reacted with a S^{2-} ion to form Cu_2S. DEG served as both reducing agent and solvent in the polyol process.

The UV-Vis DRS spectra of T-ZnO whiskers and the nanocomposites with different Cu/Zn molar ratio are shown in Fig. 5. These revealed a change of the optical absorption property of T-ZnOw after Cu_2S nanoparticles were deposited on it. The band gap energy (E_g) of the samples was determined according to the equation, $E_g = 1239.8/\lambda_g$ [3], where λ_g is the wavelength of the optical absorption edge obtained from the intersection of the two tangents of the absorption curve. As shown in Fig. 5, there was only a UV

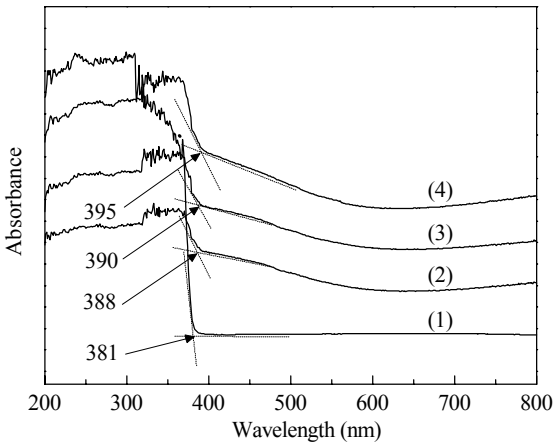

Fig. 5. UV-Vis DRS spectra of T-ZnOw (1) and Cu_2S/T-ZnOw photocatalysts with 2% (2), 4% (3), and 8% (4) Cu/Zn molar ratio.

absorption band at 381 nm (E_g = 3.25 eV) for pure T-ZnOw, which corresponded to the band gap energy of bulk ZnO. The absorption edges of the Cu_2S/T-ZnOw nanocomposites with 2%, 4%, and 8% Cu/Zn molar ratio were shifted to longer wavelengths of 388, 390, and 395 nm, respectively, and the corresponding band gap energies were 3.20, 3.18, and 3.14 eV. Moreover, the DRS spectra of the samples showed a broad absorption band between 400 and 800 nm, which may be attributed to the deposition of Cu_2S nanoparticles on the surface of T-ZnOw. The DRS result demonstrated that the Cu_2S/T-ZnOw nanocomposites have more suitable optical absorption thresholds as compared to T-ZnOw.

2.3 Photocatalytic activity

The photocatalytic activity was evaluated by the photocatalytic degradation of MO under UV light irradiation. Figure 6 shows the absorbance spectra of the MO aqueous solution with the 4% Cu_2S/T-ZnOw photocatalyst at differ-

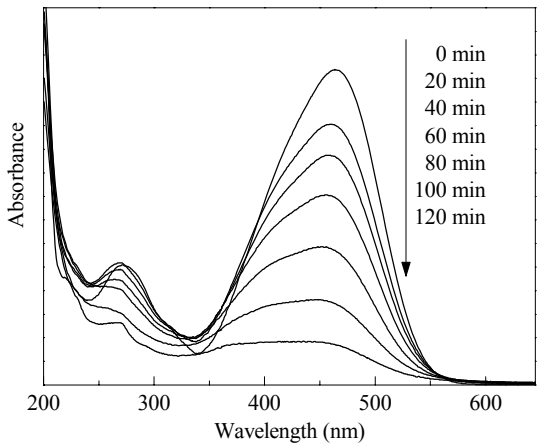

Fig. 6. Absorption spectrum changes of the MO aqueous solution with the 4% Cu_2S/T-ZnOw photocatalyst.

ent irradiation time. The absorption peak of MO at λ = 466 nm gradually decreased with irradiation time and had almost disappeared after being irradiated for 120 min, which was attributed to the demethylation and hydroxylation of MO during the photocatalytic process [7].

Figure 7(a) shows the photocatalytic degradation curves of MO with T-ZnOw and Cu_2S/T-ZnOw photocatalysts. The photodegradation efficiency (R_d) was defined as $R_d = (C_0–C_t)/C_0$ [31], where C_0 is the initial concentration of MO solution and C_t is the concentration of MO solution after irradiation time t. The photodegradation efficiency without any photocatalyst was negligible after 120 min.

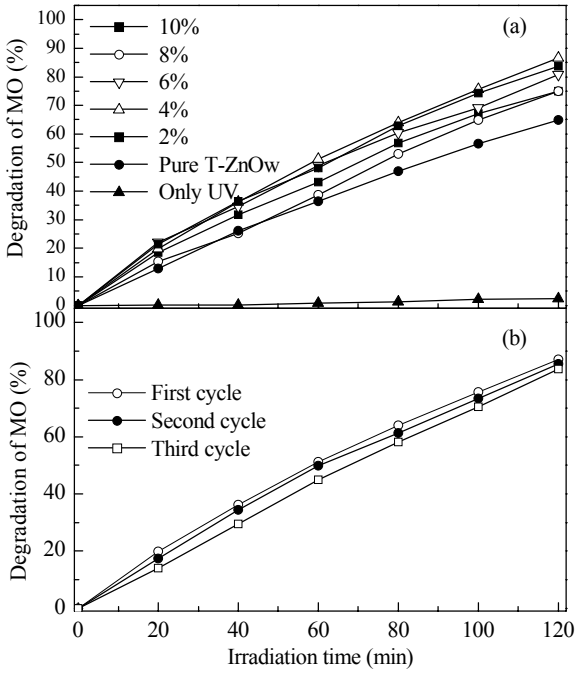

Fig. 7. Photocatalytic activity of Cu_2S/T-ZnOw photocatalysts with different Cu/Zn molar ratios (a) and the sample with Cu/Zn molar ratio of 4% after different cycles (b).

Cu_2S/T-ZnOw photocatalysts exhibited better photocatalytic activity than T-ZnOw after 120 min. The photodegradation efficiency increased with the increase of Cu/Zn molar ratio up to 4%. With further increase of the Cu/Zn molar ratio, the photodegradation efficiency decreased.

The enhanced photocatalytic activity may be ascribed to the increased hetero-junction between Cu_2S and T-ZnOw in the coupled Cu_2S/T-ZnOw photocatalysts [32]. For the coupled Cu_2S/T-ZnOw photocatalyst with different Cu/Zn molar ratios, since the yield increased with Cu/Zn molar ratio, it is reasonable to deduce that the amount of hetero-junction increased as well [2,32]. However, further increase of Cu/Zn molar ratio to 6%–10% resulted in the formation of agglomerates of Cu_2S nanoparticles and subsequently reduced the number of hetero-junctions between Cu_2S and T-ZnOw. As a result, the sample with 4% Cu/Zn molar ratio exhibited the highest photodegradation activity with a degradation rate of MO of 87% under UV irradiation for 120 min. To further investigate the stability of the catalyst, recycling experiments for degrading MO under UV light irradiation were performed. Figure 7(b) shows the change of photodegradation efficiency from the first cycle to the third cycle using 4% Cu/Zn molar ratio. The photocatalytic activity of the sample did not decline after the third cycle, which demonstrated that the photocatalyst possessed excellent stability.

It is well known that the hydroxyl radical (•OH) generated in the photocatalytic process is an extremely strong and non-selective oxidizing agent (E^0 = + 3.06 V) of organic chemicals [33,34]. Figure 8 shows the concentration of •OH determined by the reaction between •OH and $Fe(phen)_3^{2+}$ for Cu_2S/T-ZnOw photocatalyst [35]. As shown in Fig. 8, during the first 20 min, little •OH was generated in the solution and the differences in •OH concentration of the samples were relatively small, so there was little difference in the photocatalytic activity of the samples. With increasing irradiation time (60 and 120 min), more •OH was generated and

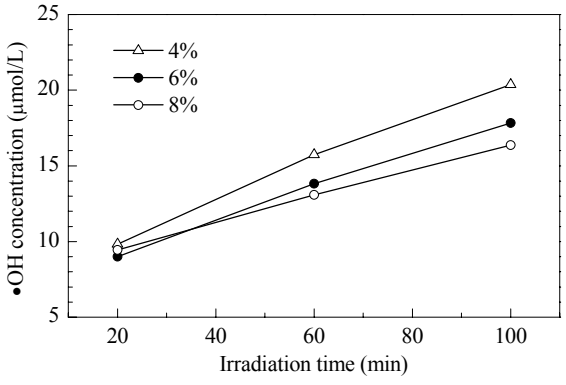

Fig. 8. The •OH concentrations in the MO aqueous solution under different UV irradiation time in the presence of the samples prepared with 4%, 6%, and 8% Cu/Zn molar ratio, respectively.

the differences in •OH concentration among the samples became larger. In particular, the concentration of •OH in the solution with the sample with 4% Cu/Zn molar ratio was higher than that of the other samples (6% and 8% Cu/Zn molar ratio), which resulted in a clear difference in the photocatalytic properties of the samples.

In summary, hydroxyl radicals play an important role in the photocatalytic process and react with adsorbed MO molecules to oxidatively decomposed them [36]. The photocatalyst with Cu/Zn molar ratio of 4% had the best activity. With the further increase of the Cu/Zn molar ratio, the photocatalytic activity decreased, which was because more Cu_2S agglomerates were formed on the surface of T-ZnOw. Cu_2S agglomerates act as recombination centers for photogenerated electrons and holes and resulted in a lower photocatalytic activity of Cu_2S/T-ZnOw.

3 Conclusions

Cu_2S/T-ZnOw nanocomposites were successfully synthesized by the polyol process using DEG as both reducing agent and solvent. The Cu_2S/T-ZnOw nanocomposites gave better optical absorption performance than T-ZnOw. The photocatalytic degradation of methyl orange revealed that the catalysts were more active than T-ZnOw. The enhanced photocatalytic activity was ascribed to increased hetero-junctions between Cu_2S and T-ZnOw in the coupled Cu_2S/T-ZnOw photocatalysts, which enhanced the separation of photogenerated electrons and holes and the photocatalyst has good potential application for environmental purification.

References

1 Hoffmana M R, Martin S T, Choi W, Bahneman D W. *Chem Rev*, 1995, **95**: 69
2 Linsebigler A L, Lu G Q, Yates J T Jr. *Chem Rev*, 1995, **95**: 735
3 Li X B, Wang L L, Lu X H. *J Hazard Mater*, 2010, **177**: 639
4 Sakthivel S, Neppolian B, Shankar M V, Arabindoo B, Palanichamy M, Murugesan V. *Sol Energy Mater Sol Cells*, 2003, **77**: 65
5 Khodja A A, Sehili T, Pilichowski J F, Boule P. *J Photochem Photobiol A*, 2001, **141**: 231
6 Gu C D, Cheng C, Huang H Y, Wong T L, Wang N, Zhang T Y. *Crystal Growth Des*, 2009, **9**: 3278
7 Chen T W, Zheng Y H, Lin J M, Chen G N. *J Am Soc Mass Spectrom*, 2008, **19**: 997
8 Mansilla H, Villasenor J, Maturana G, Baeza J, Freer J, Duran N J. *J Photochem Photobiol A*, 1994, **78**: 267
9 Ohnishi H, Matsumura M, Tsubomura H, Iwasaki M. *Ind Eng Chem Res*, 1989, **28**: 719
10 Wang J, Fan X M, Tian K, Zhou Z W, Wang Y. *Appl Surf Sci*, 2011, **257**: 7763
11 王存, 王鹏, 徐柏庆. 催化学报 (Wang C, Wang P, Xu B Q. *Chin J Catal*), 2004, **25**: 967
12 Wang C, Wang X M, Xu B Q, Zhao J C, Mai B X, Peng P A, Sheng G Y, Fu J M. *J Photochem Photobiol A*, 2004, **168**: 47
13 余长林, 杨凯, 舒庆, Yu J C, 操芳芳, 李鑫. 催化学报 (Yu C L, Yang K, Shu Q, Yu J C, Cao F F, Li X. *Chin J Catal*), 2011, **32**: 555
14 Sakthivel S, Geissen S U, Bahnemann D W, Murugesan V, Vogelpohl A. *J Photochem Photobiol A*, 2002, **148**: 283
15 Li D, Haneda H. *J Photochem Photobiol A*, 2003, **160**: 203
16 Spanhel L, Weller H, Henglein A. *J Am Chem Soc*, 1987, **109**: 6632
17 Rolison D R. *Science*, 2003, **299**: 1698
18 Arai T, Yanagida M, Konishi Y, Iwasaki Y, Sugihara H, Sayama K. *J Phys Chem C*, 2007, **111**: 7574
19 Gorai S, Ganguli D, Chaudhuri S. *Mater Chem Phys*, 2004, **88**: 383
20 Xu Y, Schoonen M A A. *Am Miner*, 2000, **85**: 543
21 Fan X M, Zhou Z W, Wang J, Tian K. *Trans Nonferrous Met Soc Chin*, 2011, **21**: 2056
22 Yin Y, Alivisatos A P. *Nature*, 2005, **437**: 664
23 Xu W, Wang Y, Bai X, Dong B, Liu Q, Chen J S, Song H W. *J Phys Chem C*, 2010, **114**: 14018
24 Sun Y G, Gates B, Mayers B, Xia Y N. *Nano Lett*, 2002, **2**: 165
25 Wagner C D, Riggs W M, Davis L E, Moulder J F, Muilenberg G E eds. Handbook of X-Ray Photoelectron Spectroscopy. Eden Prairie: Perkin-Elmer, 1979
26 Zhang X, Guo Y G, Zhang P Y, Wu Z S, Zhang Z J. *Mater Lett*, 2010, **64**: 1200
27 Ai Z H, Zhang L H, Lee S C, Ho W K. *J Phys Chem C*, 2009, **113**: 20896
28 Li S, Wang H Z, Xu W W, Si H L, Tao X J, Lou S Y, Du Z L, Li L S. *J Colloid Interf Sci*, 2009, **330**: 483
29 Rodriguez J A, Jirsak T, Chaturvedi S, Kuhn M. *Surf Sci*, 1999, **442**: 400
30 Peng M, Ma L L, Zhang Y G, Tan M, Wang J B, Yu Y. *Mater Res Bull*, 2009, **44**: 1834
31 Wang R H, Xin J H Z, Yang Y, Liu H F, Xu L M, Hu J H. *Appl Surf Sci*, 2004, **227**: 312
32 Tennakone K, Bandara J. *Appl Catal A*, 2001, **208**: 335
33 Yatmaz H C, Akyol A, Bayramoglu M. *Ind Eng Chem Res*, 2004, **43**: 6035
34 Daneshvar N, Salari D, Khataee A R. *J Photochem Photobiol A*, 2004, **162**: 317
35 Xu X L, Zhou Z W, Zhu W J. *Mater Sci Forum*, 2009, **610–613**: 229
36 Rajeshwar K, Osugi M E, Chanmanee W, Chenthamarakshan C R, Zanoni M V B, Kajitvichyanukul P, Krishnan-Ayer R. *J Photochem Photobiol C*, 2008, **9**: 171